MATERIALS SCIENCE

# Harnessing the duality of bases toward controlled color and fluorescence

**Dingbowen Wang[1,2,3], Yi Wang[4], Tawanda J. Zimudzi[5], Long-Qing Chen[4], Jian Yang[1,2,3]***

**Bases can promote keto-enol tautomerism, a prevalent form of prototropic tautomerism, and facilitate the ring opening of anhydride ring structures. The intrinsic chemical distinctions between these processes provide an opportunity to modulate these seemingly parallel reactions. However, this potential remains largely unexplored. In this work, we report homophthalic anhydride, the first molecule exhibiting simultaneous halochromism, turn-on fluorescence (halofluorochromism), and subsequent self-destruction. Through comprehensive spectroscopic analysis and theoretical calculations, we unravel the mechanisms underlying these phenomena, revealing that the pivotal roles of the base's basicity and nucleophilicity specifically allow us to achieve controlled durations of color change and turn-on fluorescence. Capitalizing on these intriguing properties, we develop a highly dynamic CMY (cyan-magenta-yellow) palette ideal for entity encryption and anti-counterfeiting applications. Our work reshapes the understanding of the relationship between the basicity and nucleophilicity of bases, enriching the comprehension of keto-enol tautomerism and homophthalic anhydride chemistry, and unveils a spectrum of potential applications.**





## INTRODUCTION

Keto-enol tautomerism stands as a cornerstone in organic chemistry, denoting the equilibrium between ketones (or aldehydes) and their isomeric enol counterparts. Facilitated by a hydrogen atom adjacent to a carbonyl group, this equilibrium hinges on intramolecular proton transfer (*1*, *2*). The position of this equilibrium can be influenced by factors such as solvent, pH, temperature, and the nature of the substituents (*1*, *3*–*8*). This tautomerism finds applications in pharmaceutical design, elucidation of enzymatic reaction mechanisms, and synthesis of intricate organic compounds (*1*, *2*, *9*–*14*). For instance, the enol form acts as a nucleophile in the aldol reaction, a fundamental step in many synthetic pathways (*15*–*17*). Moreover, the tautomeric equilibrium has been extensively studied in relation to the stability and reactivity of biomolecules like DNA bases and proteins, highlighting the biological significance of this phenomenon (*10*–*12*, *18*–*20*). Six-membered anhydride ring structures, distinct from the more commonly encountered five-membered cyclic anhydrides, are rarer in nature and synthesis due to their unique reactivity, offering insights into ring size effects on chemical stability and reactivity (*21*–*23*). When the six-membered anhydride ring and keto-enol tautomerism encounter bases, they both undergo a structural change but with distinct chemical natures. For keto-enol tautomerism, a base abstracts the α-hydrogen and facilitates the transition from keto form to enol form, depending on its basicity, whereas for breaking up anhydride ring, the base attacks at the carbonyl carbon as a nucleophile. This leaves a space to control the tautomerization and ring opening separately. However, there is currently a lack of studies on the correlation between the duality of bases and the keto-enol tautomerism and six-membered anhydride ring–related structural changes. In this work, we elucidate the underlying mechanisms of the pH-induced color change and turn-on fluorescence (together termed halofluorochromism) as well as self-destruction of a model molecule, homophthalic anhydride (HA), and investigate how the basicity and nucleophilicity of a base affect the corresponding structural changes. By decoupling the basicity and nucleophilicity, we achieved controlled duration of halofluorochromism or, in other words, self-destruction time. Empowered by the intriguing characteristics of HA and the duality of bases on HA, we develop a cyan-magenta-yellow (CMY) palette with dynamic multidimensional and multimode optical encryption features for information encryption and anti-counterfeiting. Our findings thereby contribute to the design of dynamic molecules and materials with tunable color and fluorescence changes and more potential fields.

## RESULTS

### Halofluorochromism and tunable self-destruction of HA

The pH-induced color change (halochromism) phenomenon of HA was observed serendipitously during our organic synthesis trials with HA and basic compounds accompanied by the subsequent discovery of its turn-on fluorescence. As depicted in Fig. 1 (A to D), HA displayed a halofluorochromic behavior. In the absence of a base, the HA solution remained colorless, showing neither absorption nor fluorescence emission in the visible spectrum. However, upon base addition, prominent peaks emerged at 433 nm for absorption (yellow color) and 534 nm for fluorescence, marking a stark transition from "off" to "on." Intriguingly, both the yellow color and the yellow-green fluorescence of the solution were transient, diminishing over time (Fig. 2, A and B; the blue fluorescence observed in Fig. 2A originates from the ester formed in the subsequent reaction, which will be discussed in later sections). For instance, when 100 μl of pure 1,8-diazabicyclo(5.4.0)undec-7-ene (DBU) or triethylamine (TEA) was added to 2.5 ml of a 1 mM HA solution in acetonitrile, the yellow color dissipated to some extent within a timescale of tens of minutes, and when concentrated NaOH was added, the yellow color faded even more rapidly, at a rate visible to the naked eye.

[1]School of Engineering, Westlake University, Hangzhou, Zhejiang 310030, China. [2]Research Center for Industries of the Future, Westlake University, Hangzhou, Zhejiang 310030, China. [3]Department of Biomedical Engineering, The Pennsylvania State University, University Park, PA 16802, USA. [4]Department of Materials Science and Engineering, The Pennsylvania State University, University Park, PA 16802, USA. [5]Materials Research Institute, The Pennsylvania State University, University Park, PA 16802, USA.
*Corresponding author. Email: yangjian07@westlake.edu.cn

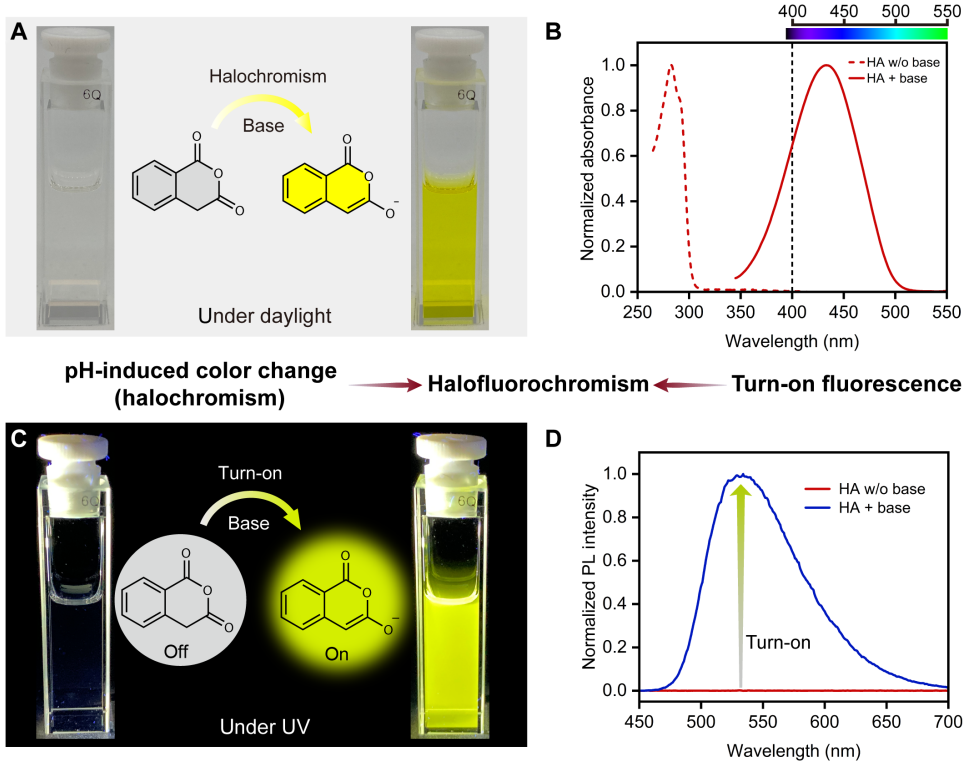


**Fig. 1. Halofluorochromism behavior of HA.** (**A**) pH-induced color change (halochromism) behavior of HA. Upon base addition, the colorless HA solution turns to yellow color. (**B**) Upon base addition, the absorption peak of HA shifts from 283 to 433 nm. (**C**) pH-induced turn-on fluorescence behavior of HA. Upon base addition, the colorless HA solution emanates yellow-green fluorescence under UV light. (**D**) Upon base addition, the HA solution exhibits complete "turn-on" fluorescence and emits a pronounced yellow-green fluorescence with a peak wavelength at 534 nm.

To explain this behavior, we put forth a mechanism, which is rooted in the chemical structure of HA, as illustrated in part of Fig. 2C. HA, before adding the base (the keto form of HA, $HA_k$), features a benzene ring in tandem with a six-membered anhydride ring, which is not fully conjugated. We unexpectedly found that there is a lack of single-crystal data of $HA_k$ in literature or any database. So, we conducted single-crystal x-ray diffraction experiment on $HA_k$ and deposited it in Cambridge Crystallographic Data Centre (CCDC) under a new CCDC number: 2206140. The single-crystal x-ray diffraction data clearly present a nonplanar configuration for the anhydride ring of $HA_k$. In detail, the dihedral angles are 3.5° for C4-C7-C8-O9, 7.8° for C5-C10-O9-C8, and 8.5° for C7-C8-O9-C10 in contrast to those from the benzene ring (all less than 0.5°), confirming its nonconjugated structure (Fig. 2, D and E, and table S1). As a result, the absorption of $HA_k$ falls into the ultraviolet (UV) range and no fluorescence can be observed. When a base is introduced, the α-methylene ketone moiety of HA undergoes keto-enol tautomerization, transforming into an enolate (the enolate form of HA, $HA_e$). This transition engenders a fully conjugated ring structure, yielding a D-π-A push-pull structure where the remaining carbonyl group works as the electron-withdrawing group and the newly formed enolate is a strong electron-donating group. The rigid planar structure endows $HA_e$ with bright fluorescence, and both conjugated system extension and the newly formed D-π-A push-pull structure are attributed to the bathochromic shift of absorption and fluorescence of HA. Furthermore, the base serves a dual role: It aids in α-hydrogen abstraction, driving keto-enol tautomerization, and also partakes in nucleophilic attacks on the carbonyl carbon on the other side of the anhydride ring (Fig. 2F). This dual action, on the one hand, leads to a keto-to-enolate transformation that endows HA with a yellow color and yellow-green turn-on fluorescence; on the other hand, it induces ring opening, which causes the color and fluorescence to wane over time.

To dissect the underlying mechanisms of the halofluorochromic behavior and the associated fading, we sought to obtain relative long-lived yellow-colored molecular species for some characterizations such as UV-visible absorption (UV-vis), fluorescence, and nuclear magnetic resonance (NMR) spectroscopies. Given that the enolization and deprotonation of the α-methylene ketone part of HA resulting in the color change are contingent on the basicity of the base, while the ring opening that brings self-destructive behavior hinges on the nucleophilicity, it is interesting to investigate whether the halofluorochromic and the self-destructive behavior of HA could be decoupled and controlled by adjusting the basicity and nucleophilicity of the base. In most cases, the base with stronger basicity also has stronger nucleophilicity. However, there are several non-nucleophilic bases that exist (note S1, both nucleophilic and non-nucleophilic bases used or mentioned in this work are summarized in table S2). Thus, we predicted that the non-nucleophilic base could still convert HA from the keto form to its enolate form by abstracting the α-hydrogen while effectively preventing the ring opening from the nucleophilic attack. In other words, the persistence of

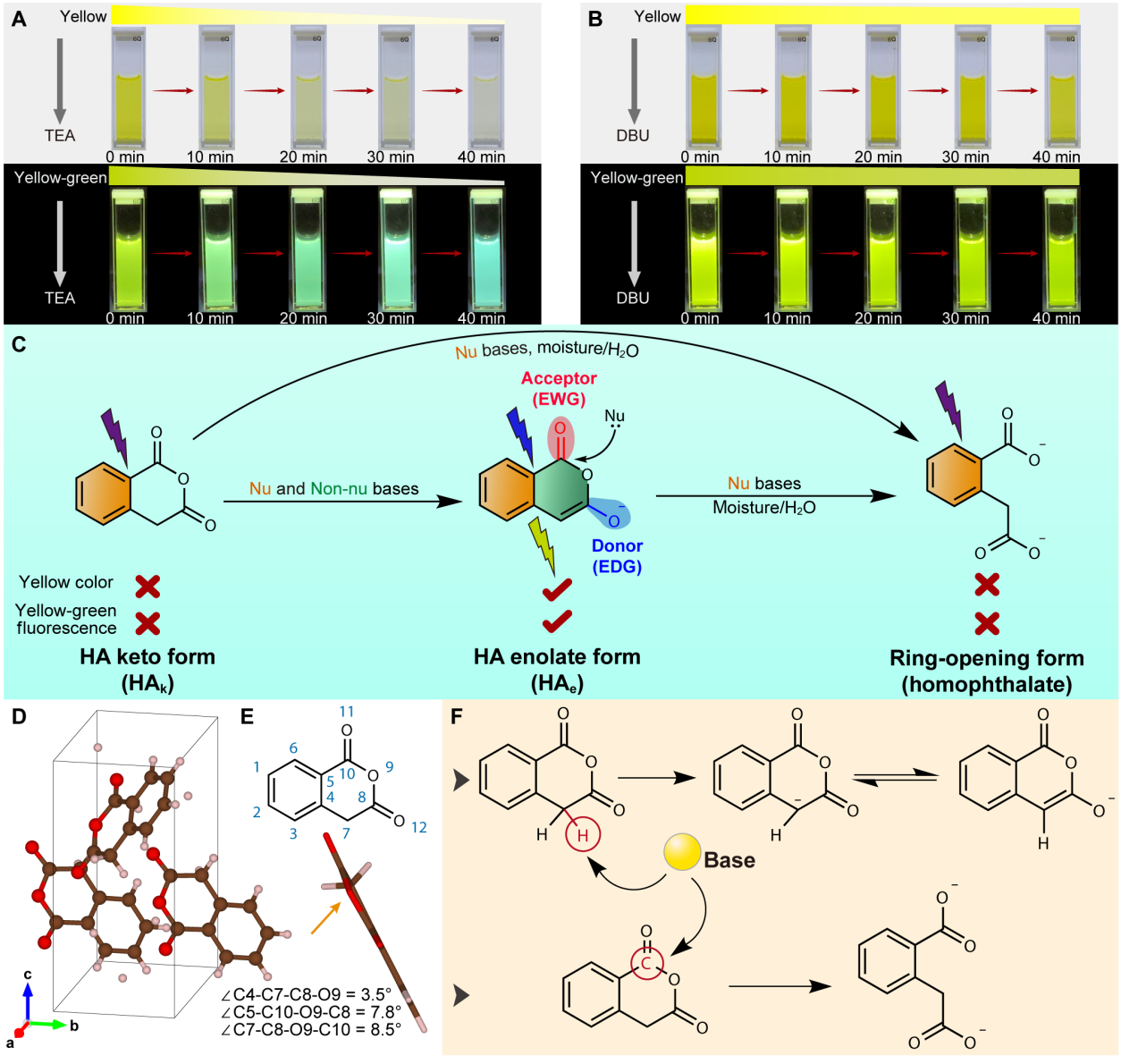


**Fig. 2. Self-destruction behavior of HA.** (**A**) Photos of decay progress of HA after adding TEA. Upon addition of nucleophilic base, TEA, the yellow color and yellow-green fluorescence diminished over time (the blue fluorescence originates from the ester formed in the subsequent reaction, which will be discussed in later sections; we only focus on the yellow-green fluorescence from $HA_e$ here). (**B**) Photos of decay progress of HA after adding DBU. Upon addition of non-nucleophilic base, DBU, the yellow color and yellow-green fluorescence decayed much slower. (**C**) Proposed mechanisms of the halofluorochromism and self-destruction behaviors of HA. (**D**) Single-crystal unit cell of $HA_k$ (C, brown balls; O, red balls; and H, white balls). (**E**) Stick model of $HA_k$ (the out-of-plane structure is manifested by the 3.5° C4-C7-C8-O9, 7.8° C5-C10-O9-C8, and 8.5° C7-C8-O9-C10 dihedral angles). (**F**) Scheme illustrating the duality of bases on keto-enol tautomerization and anhydride ring opening of HA.

$HA_e$, along with its yellow hue and turn-on fluorescence, can be modulated by manipulating the base's nucleophilicity while maintaining strong enough basicity.

Upon addition of a non-nucleophilic base, DBU, both the yellow color and the turn-on fluorescence exhibited a significantly prolonged duration compared to that of nucleophilic counterpart, as shown in Fig. 2 (A and B). This observation supports our hypothesis that the halofluorochromism and self-destruction of HA can be independently controlled by harnessing the duality of bases. Therefore, the complete hypothesis was that $HA_k$ can be converted to $HA_e$, which has both yellow color and turn-on fluorescence, by adding either nucleophilic or non-nucleophilic bases, whereas $HA_k$ and $HA_e$ can only transform into the ring-opening form, homophthalate, upon the addition of nucleophilic bases, resulting in the loss of both the yellow hue and the yellow-green fluorescence (Fig. 2C).

UV-vis and fluorescence spectroscopies were then conducted to interrogate the photophysical properties of HA. The spectroscopic features have been mentioned above. Just note that the large absorption redshift (150 nm) indicated the existence of another mechanism besides conjugated system extension, such as intramolecular charge transfer (ICT), which further extends the absorption wavelength. Furthermore, the quantum yield of $HA_e$ in acetonitrile was

determined to be around 5.51% (note S2 and fig. S1) and solvent polarity effect on photophysical properties of $HA_e$ was also investigated (fig. S2). Next, the absorption and fluorescence decay profiles with different base addition were recorded at fixed wavelengths to monitor the dynamic change of the chromogenic/fluorogenic species in the solution. Upon addition of a nucleophilic base, TEA, the absorption and fluorescence emission intensity decreased rapidly, while, after adding DBU, the decay rates were much slower (Fig. 3, A and B, and fig. S3). Of note, the absorption and fluorescence decay curves of HA after adding DBU matched well. It was observed that 44.3% of the original absorbance (at 430 nm) and 42.5% of fluorescence intensity (at 530 nm) remained 2 hours after DBU addition, which are close to each other, indicating that the same chemical species contributed prominently to the yellow color and fluorescence. In contrast, the absorption decay curve of HA after adding TEA was apparently above the fluorescence decay curve. It was observed that 25.6% of the original absorbance but only 9.8% of fluorescence intensity remained 2 hours after TEA addition (fig. S4). The above results imply that more complicated chemical reactions occurred in the solution when adding TEA than after adding DBU, and some chemical species only formed in the solution with TEA, contributing to the difference between absorbance and fluorescence intensity reduction. Besides, the absorption and fluorescence decay profiles show that the degradation of $HA_e$ may have different reaction orders and merits for a further investigation.

Kinetic measurements of Fourier transform infrared (FTIR) spectroscopy were then applied. As shown in Fig. 3C, before adding the base, two peaks were observed at 1803 and 1754 $cm^{-1}$, which correspond to the two carbonyls of the keto form of HA, and the shoulder at 1728 $cm^{-1}$ is consistent with the carboxylic C═O of homophthalic acid (*24*), indicating a small degree of conversion of HA to the diacid. Upon addition of DBU, the two anhydride C═O peaks

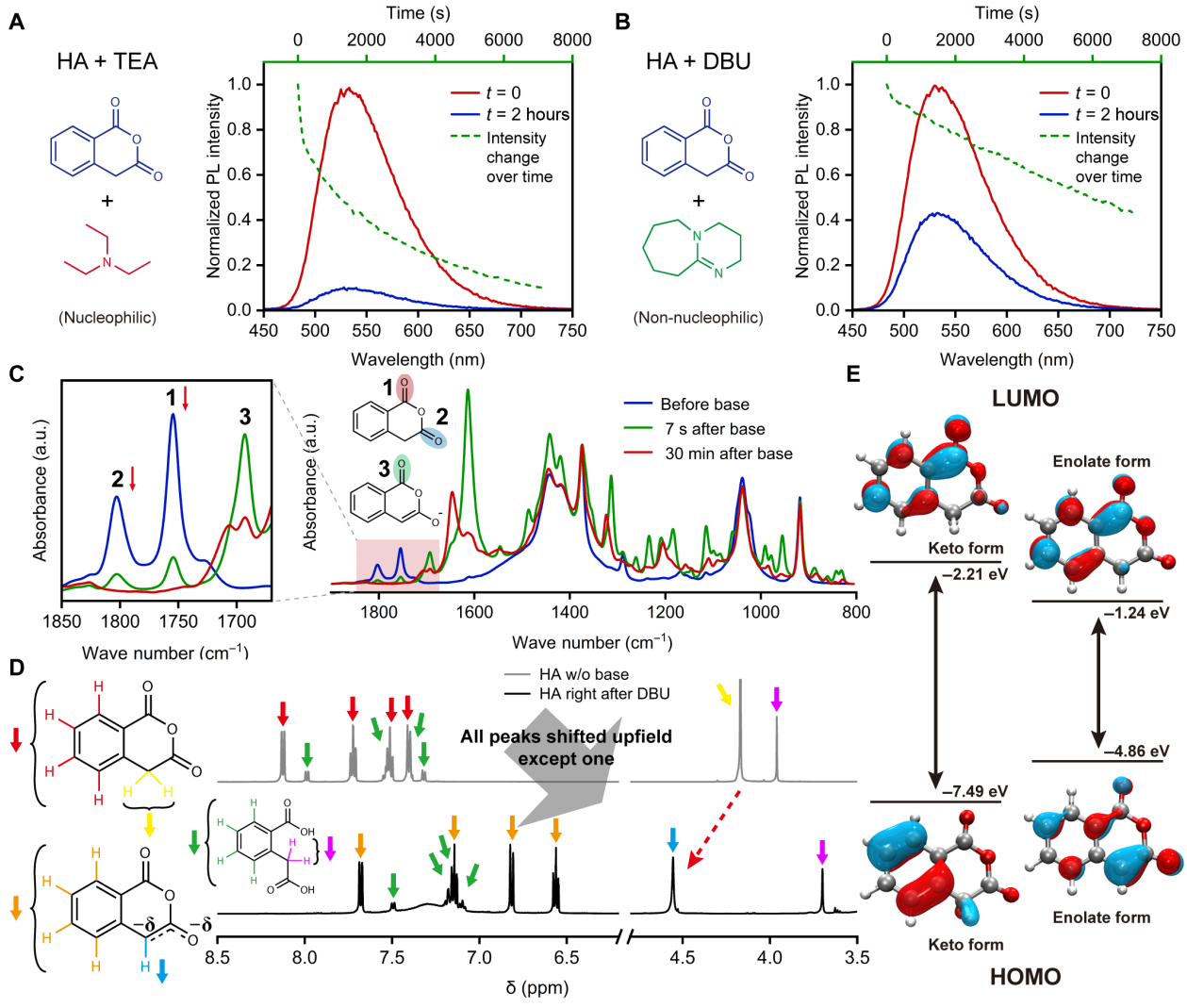


**Fig. 3. Mechanistic studies and structure characterizations of HA upon adding different bases.** (**A**) Fluorescence emission spectra of HA right after and after 2 hours of adding TEA ($\lambda_{ex}$ = 430 nm) and the intensity change profile over time plot ($\lambda_{ex}$ = 430 nm, $\lambda_{em}$ = 530 nm). (**B**) Fluorescence emission spectra of HA right after and after 2 hours of adding DBU ($\lambda_{ex}$ = 430 nm) and the intensity change profile over time plot ($\lambda_{ex}$ = 430 nm, $\lambda_{em}$ = 530 nm). (**C**) FTIR spectra of HA before, after 7 s, and after 30 min of adding DBU. (**D**) NMR spectra of HA before and after adding DBU. (**E**) Calculated bandgap and electron distribution for the HOMO and LUMO of $HA_k$ and $HA_e$.

rapidly diminished then disappeared, and a peak at 1693 $cm^{-1}$ appeared, which is assigned to C═O vibration from the enolate form of HA. This C═O peak reached its maximum in seconds and then continued to decrease, indicating that the degradation of the enolate form of HA was proceeding. The decrease of the C═N peaks of DBU at 1614 and 1315 $cm^{-1}$, along with the emergence of C═$NH^+$ peaks at 1646 and 1324 $cm^{-1}$, suggests proton abstraction by DBU. The peak pattern changes in the TEA group are similar to those observed with DBU, both showing a decrease in $HA_k$ and an increase in $HA_e$. Note that one peak at ~1706 $cm^{-1}$, observed in spectra after adding either DBU or TEA and contributed to C═O, aligns with the partial double-bond characteristic of the enolate moiety, as confirmed by the NMR data below. The detailed data analysis and additional FTIR spectra can be found in the Supplementary Materials (note S3 and figs. S5 to S8).

NMR spectroscopy was exploited to further investigate the detailed chemical structure information and reaction mechanisms. Kinetic measurements of HA samples after adding DBU and TEA presented dynamic changes of chemical species and exhibited more complex reactions in TEA than those in DBU. On the basis of the $^1H$ spectra of HA shown in Fig. 3D, the group of small peaks (green and magenta arrows in Fig. 3D) were assigned to the ring-opening form, homophthalic acid, indicating that there was a small portion of HA already hydrolyzed before adding the base, probably due to the air moisture as confirmed by the FTIR results. Comparing the $^1H$ spectra of HA before and after adding the base, almost every peak shifted upfield except one; the overall shifts could be ascribed to the pH effect, while the peak at 4.17 parts per million (ppm) was contrary to the trend and shifted downfield to 4.56 ppm. This proposed enolic CH exhibited chemical shifts of 4.56 ppm ($^1H$) and 73.69 ($^{13}C$) ppm, which are between the conjugated vinylic and saturated proton/carbon chemical shift range. These chemical shifts clearly showed that the proposed enolate part of HA is ambident, referring to the negative charge being delocalized over the α carbon and the oxygen, endowing all bonds among the enolate region partial double-bond character, which is in accordance with the literature for similar molecules and common chemical knowledge (*25*, *26*). Although mentioned explicitly or vaguely in previous literature on HA (*27*–*29*), our NMR results are the first definite evidence of the formation of an enolate structure from HA in basic environments. The $^1H$ and $^{13}C$ chemical shifts combined with two-dimensional spectra of HA right after adding DBU provide solid proof of the structural change from $HA_k$ to $HA_e$. While in the solution with added TEA, $HA_e$ can react with homophthalate, either from the small amount in the starting materials or from the ring opening of HA by nucleophilic attack of TEA, to form an ester, resulting in the aforementioned rapid decrease of absorbance and yellow-green fluorescence intensity. With the help of $^1H$, $^{13}C$, distortionless enhancement by polarization transfer NMR experiments and chromatographic purification, the structure of the ester product in TEA reaction was elucidated. All NMR spectra, the detailed analysis, and discussions are in note S4 and figs. S9 to S19.

Putting the spectroscopic data together, the commercial HA sample used as received initially contains a small portion of homophthalic acid. The addition of nucleophilic base, TEA, results in the enolate form and ring-opening form of HA followed by rapid esterification, and thus, the enolate form, as well as the yellow color and yellow-green fluorescence, quickly depletes. The formed ester exhibits a certain degree of blue fluorescence (fig. S20), as previously mentioned. The addition of non-nucleophilic base, DBU, makes the enolate form of HA much stabler and it lasts for a much longer time, and the enolate part of HA exhibits a partial double-bond characteristic where the negative charge is delocalized over the α carbon and the oxygen (fig. S21). High-resolution mass spectrometry spectra of $HA_e$, homophthalate, and the ester were successfully collected (figs. S46 to S48), further supporting the above mechanisms. A scheme of proposed whole reaction mechanisms between HA and TEA (nucleophilic base) or DBU (non-nucleophilic base) is shown in fig. S21.

To better understand the photophysical changes and reaction mechanisms, we performed first-principles calculations based on time-dependent density functional theory (DFT) (Fig. 3E, figs. S49 to S51, and note S5). The calculated HOMO (the highest occupied molecular orbital)–LUMO (the lowest unoccupied molecular orbital) gap and the calculated strongest absorption wavelength (271.59 nm) for $HA_k$ and (412.65 nm) for $HA_e$ are in agreement with our experimentally measured absorption maxima at 283 and 433 nm, respectively. The calculated electron density distribution diagrams of HOMO and LUMO align with the hypothesized structural alteration. The results support the fact that $HA_e$ has a higher degree of conjugation. The transition from $HA_k$ to $HA_e$ markedly elevates the electron charge density in the right-side ring, accompanied by a denser electron cloud correlation at the enolate part, signifying the augmented conjugation of the ring and electron delocalization across the enolate moiety. Notably, the transition dipole calculated for $HA_e$ (2.523 D) is significantly higher than that of $HA_k$ (1.437 D), suggesting that upon photoexcitation, $HA_e$ exhibits a more significant dipole moment. This finding, combined with their excited charge density difference between the ground state ($S_0$) to the first excited state ($S_1$), supports the proposed ICT process in $HA_e$.

## Dynamic CMY palette for encryption and anti-counterfeiting

An information encryption system can be simplified as three integrated components: the input, the material, and the output (*30*, *31*). The fewer materials integrated, the simpler and more reliable the system is, whereas the more diverse the combination of inputs and outputs, the more secure the encryption system is. By leveraging the halofluorochromism and controlled self-destruction properties of HA, we developed a highly dynamic CMY palette for entity encryption and anti-counterfeiting. Two leuco dyes, phenolphthalein (PhPh) and α-naphtholphthalein (NaPh), were chosen as magenta and cyan colorants, while HA served as the yellow colorant. The rationale behind the choice was discussed in note S6. In theory, by altering the concentration and ratios of C, M, and Y colorants, just like a real palette, any color within the color gamut of the system can be obtained, and a continuous and seamless color tuning can be achieved. The continuous color tunability was tested, and the potential color gamut was simulated (notes S7 and S8 and figs. S25 to S30).

We subsequently applied the palette system we developed to inkjet printing and handwriting, which are the two major implementations in information encryption applications (Fig. 4A). When colorants are deposited onto a substrate, the situation differs from when they are in solution. In solution, the molecules are surrounded by solvent molecules, while when deposited on a substrate, they behave more like in a solid state and interact with the substrate surface to some extent. In general, conventional organic fluorophores, which exhibit bright fluorescence in dilute solution, suffer from aggregation-caused quenching in their solid state (*32*, *33*), hindering

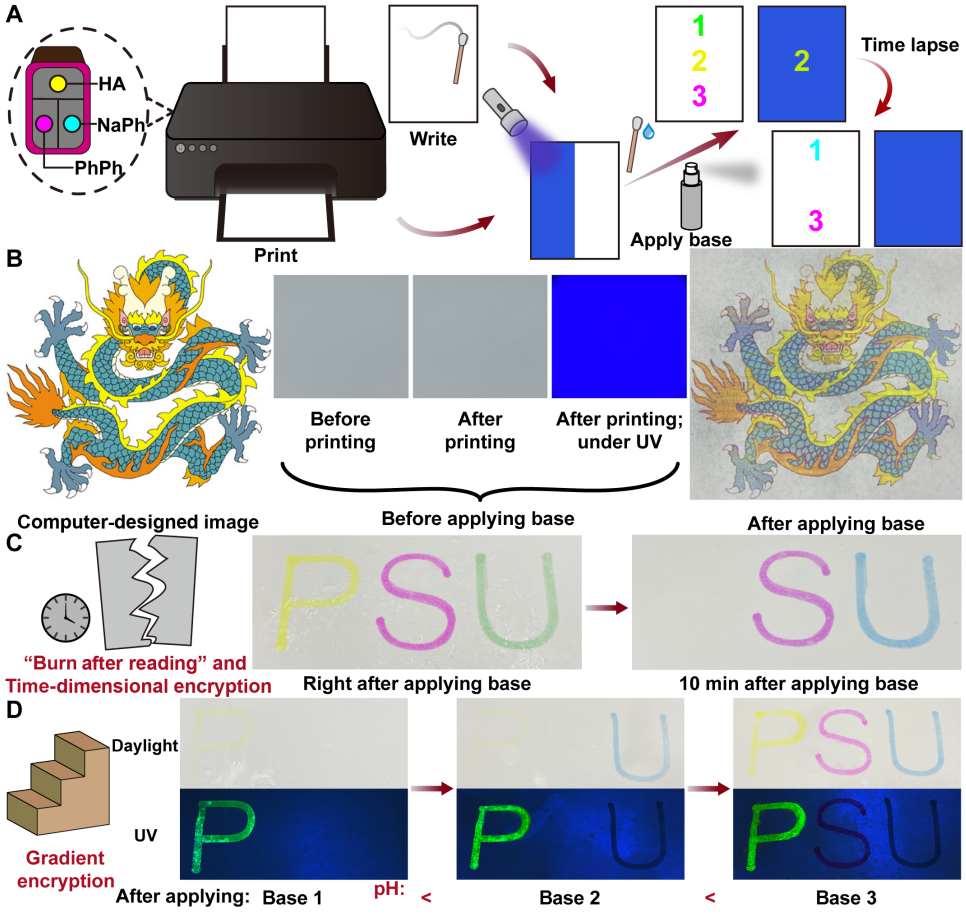


**Fig. 4. Information encryption by applying the CMY palette system.** (**A**) Schematic of encryption and security printing/writing procedures. (**B**) A Chinese dragon image printed by exploiting the CMY palette system. After printing, no ink traces could be observed under either ambient or UV light, while once the base was applied, the colored pattern appeared instantaneously. The dragon image was used with permission. (**C**) "Burn after reading" and time-dimensional encryption demonstration. Taking advantage of the metastable characteristic of $HA_e$, the HA (yellow) parts gradually disappeared after applying the nucleophilic base. (**D**) Gradient encryption demonstration. Sequentially applying the bases with the pH between the color transition points of HA, PhPh, and NaPh gradually revealed the information encrypted by the three colorants.

their applications in anti-counterfeiting and information encryption. Intriguingly, $HA_e$ exhibits bright turn-on fluorescence in both solution and solid state (on the substrate surface), which differs from conventional organic fluorophores and enables another layer of encryption.

A computer-designed Chinese dragon image was first printed on printer paper using an inkjet printer by loading pure HA (Y), PhPh (M), and NaPh (C) solutions into the corresponding chambers of a customized CMY ink cartridge (Fig. 4B and movie S1). Right after printing, the solvent in the ink drops was evaporated in seconds, leaving no noticeable ink traces under daylight and UV light. After applying the base, the image with the expected colors appeared instantly. The Chinese dragon image was then printed on a nonfluorescent inkjet paper to avoid strong background fluorescence, and it also showed that the invisible feature and only the HA (yellow)–dominant portions displayed fluorescence under UV after applying the base (fig. S31). The palette system's performance was further assessed on various substrates, with consistent results (note S9 and figs. S32 and S33). Besides the normal reflective and emissive modes of encryption, the self-destruction of HA enables an extra type of security feature: "burn after reading" and time-dimensional encryption, which means that the information or color parts written by HA will disappear after a certain amount of time after applying the base (Fig. 4C and movie S3). This allows the creation of self-destructive information suitable for time-sensitive application scenarios, such as cashing bank checks within the validity period. As shown in Fig. 4C, three letters were written with yellow (HA), magenta (PhPh), and green (HA-NaPh 1:1 mix), respectively. Right after applying the base, the yellow "P," magenta "S," and green "U" appeared, and after 10 min, the yellow parts (the whole P and yellow color of U) had already completely disappeared, leaving the magenta S and cyan U. By tuning the nucleophilicity of the base, the persistence of HA (yellow) parts can be manipulated (fig. S34). Furthermore, the different color transition points of the C, M, and Y colorants enable gradient encryption (Fig. 4D and fig. S35). By applying base 1, the yellow parts showed up; after applying base 2, the cyan parts appeared; and when base 3, which is strongest among the three bases, was applied, the magenta parts showed and the whole "PSU" could be observed. These demonstrations proved that our palette system can also be used to encode the encryption information in multiple

domains. Moreover, an exemplary case to show how to exploit our palette system in anti-counterfeiting is presented in fig. S36 and note S10.

For the potential commercialization, we tested the ink's stability under two conditions, (i) before writing and (ii) after writing but before applying the base on printer paper. Before writing [condition (i)], the solutions of three colorants were stored for 3 months, and their performance was compared by writing with inks that had been stored for 3 months or freshly prepared after applying the base and monitoring the degradation using UV-vis spectroscopy. To test the stability of the CMY ink solutions under condition (i), 100 mM HA in acetone and 10 mM PhPh and 2.5 mM NaPh in ethanol were stored in capped 15-ml tubes for 3 months. Two groups of characters, P, S, and U, were written using HA, PhPh, and NaPh solutions, respectively. In fig. S37, the upper characters were written with solutions stored for 3 months, while the lower ones were written with freshly made solutions. Upon base addition, the two groups of S and U showed no appreciable difference, while the yellow (HA) part, i.e., P made from the group stored for 3 months, exhibited a slightly lighter color than the freshly made group, which indicated some degree of degradation (fig. S37). Thus, to further quantitatively investigate the stability, UV-vis spectroscopy was applied to measure the absorption change of the three ink solutions after 3 months. As shown in fig. S38, after adding the base, the absorption of PhPh and NaPh hardly changed from freshly made to 3 months' storage, showing excellent stability of PhPh and NaPh in solution, whereas the absorption of HA decreased to around 50% after 3 months, indicating that the HA molecules were slowly degrading in solution and corresponding to the results on paper writing. The above results showed that PhPh and NaPh have excellent stability in solution, whereas the stability of HA in solution is moderate. Therefore, there is room to improve the stability of HA solution for long-term storage purposes. On the other hand, since the coloration of the HA ink before and after storage for 3 months did not show a significant difference, for some application scenarios that do not require restricted coloration effects, the long-term stored HA solution is also acceptable. In other words, the acceptable threshold of long-term storage results of HA solution depends on the specific application. Moreover, removing the moisture and air combined with sealing the container of the HA solution, increasing HA concentration, adding protective ingredients, changing the solvent, or choosing another form of HA such as dry powder might all help improve the stability of HA solution and prolong the duration of its storage.

To assess the colorant stability after being written on paper [condition (ii)], the magenta (PhPh) and cyan (NaPh) parts exhibited no significant difference up to 3 weeks, while the yellow (HA) parts were quite dim after 1 week and further disappeared completely within the second week (fig. S39). Sealing the writing area with a tape, placing the paper in a desiccator, and even putting the paper in a glovebox right after writing did not make any difference. By heating the paper to remove moisture and with the help of Attenuated total reflection Fourier-transform infrared (ATR-FTIR) spectroscopy, we confirmed that the adsorbed water/moisture from the cellulose (paper) plays a major role in the degradation of HA. The details are discussed below.

It is well known that the main component of common paper is cellulose, which is a polysaccharide consisting of repeating β-1,4–linked D-glucose units. Because of its abundant hydroxyl groups in the cellulosic fiber, the surface of paper appears hydrophilic. The hydrogen bonding is attributed to the water/moisture absorption and retention from the air (*34*). Taking oxygen atoms from intra- and intermolecular C—O—C bonds into account, the number of hydrogen bonding acceptors is more than that of hydrogen bonding donors, which enables water molecules to adsorb and be stabilized on the paper surface (fig. S40) (*35*). There are some other factors that can also appreciably affect the water adsorption capability of cellulosic fibers, including temperature of surroundings and humidity of air (*34*, *36*, *37*), and we used these two factors to help us investigate the interactions between water and HA on the paper surface.

Owing to the surface and in situ measurement capability, ATR-FTIR spectroscopy is the ideal technique to investigate the chemical changes of HA degradation on the paper surface. The 1644-$cm^{-1}$ OH bending peak is suitable for analyzing the water content of cellulose and is usually well visible considering the cellulose spectrum (*35*, *38*). Meanwhile, the OH stretching absorption band between 3700 and 3000 $cm^{-1}$, which is assigned to the intra- and intermolecular hydrogen bonding, might also provide some information on water content change (*35*). Since 2 weeks after writing, no yellow color appeared on the paper when we applied the base, and we speculated that the moisture in the air might have reacted with HA and hydrolyzed the anhydride ring, resulting in the loss of color change ability. A desiccator with bench vacuum and an argon gas glovebox were used. However, as mentioned in the main text, putting the paper in either the desiccator or glovebox did not help at all. This reminded us that there might be interactions between HA and something already on the paper surface. Considering the hydrophilic nature of cellulosic fibers, the adsorbed water on the paper surface becomes the most possible factor.

As shown in fig. S41, we first measured a blank printer paper surface. The appreciable water signal centered at 1644 $cm^{-1}$ indicated the existence of adsorbed water on the paper surface. Then, a cotton swab tipped with 100 mM HA acetone solution was used to write on the paper. Shortly after the solvent evaporated, the paper was measured. Two new distinct peaks around 1780 and 1750 $cm^{-1}$ were assigned to two carbonyl groups of HA correspondingly, while the water peak still showed up. In contrast, the written paper after 2 weeks exhibited no HA carbonyl peaks, indicating the full degradation of HA, corresponding to the observation that no yellow color appeared when applying the base. Since putting the paper in the glovebox did not prevent HA degradation, meaning that the hydrogen bonds between adsorbed water and cellulosic fibers were strong enough to withstand the extraction force from the atmosphere in the glovebox, another attempt, heating the paper to remove the adsorbed water, was exploited to prevent the hydrolysis of HA. The influence of heating on the paper was investigated (fig. S42). The paper was heated at 110°C in an oven for 10 hours. Compared to the blank, the paper right after heating showed a clear decrease of the 1644 $cm^{-1}$ water peak, and after 10 min in the ambient environment, the water peak intensity increased but remained lower than that of the blank. After 20 min, results showed no apparent difference compared to the 10-min results, and the 1644 $cm^{-1}$ peak further increased after 30 min but was still lower than that of the blank (fig. S42). The 3700 to 3000 $cm^{-1}$ band did not exhibit an informative trend. Since this broad band comprises both -OH from cellulose and water, it might result from the -OH perturbations from cellulose after the water was removed/reduced. Therefore, in agreement with the literature, we believe that the 1644 $cm^{-1}$ peak brings more reliable and solid evidence of the water content changes. We also wrote

on the heated paper and placed it in the ambient environment for 2 weeks. There was no yellow color after applying the base, and the FTIR spectrum also showed the disappearance of the two HA peaks, quite similar to that without heating (fig. S41). These results showed that (i) the heating can effectively reduce/remove the adsorbed water on the paper surface; (ii) once the paper is taken out of the oven, it will slowly absorb water/moisture again. Back to the HA degradation mechanisms study, since we know that heating can effectively reduce/remove the adsorbed water on the paper surface, this time we used a heated paper written right after putting into the glovebox and expected it to retain color change capability after 2 weeks. The experimental results perfectly met our expectations: After applying the base, the written information turned to yellow color, and the two HA peaks were conspicuous, while the adsorbed water peak remained lower than the blank (fig. S41). Conclusively, with the adsorbed water removal/reduction, the HA degradation was effectively slowed down, and this strongly supports that the adsorbed water on the paper surface plays a crucial role in the HA degradation before applying the base. On the basis of the above results, we predicted that by increasing the HA concentration in the ink, the effective time of steganographic information could be prolonged. After increasing the HA concentration from 100 to 500 mM, the yellow color was still quite noticeable after 2 weeks even though slightly dimmer (fig. S43). To sum up, the C, M, and Y inks are quite stable in solution; C and M colorants are also stable for up to 3 weeks after being written on the printer paper, while Y colorant (HA) keeps decaying over time once written on the paper. This results in an effective time of the information before applying base, and it can be manipulated by tuning the concentration of HA.

Furthermore, we developed a smartphone app to enhance anticounterfeiting measures, enabling the detection of subtle color variations often overlooked by the human eye, thereby leveraging the continuous color tuning capability of our palette system (movie S4). Last, putting the aforementioned capabilities of the palette system all together, a schematic illustration of the workflow and all encryption features of the palette system are given in fig. S44.

## DISCUSSION

Currently, we have only investigated and observed that as the amount of the base added increases within a certain range, the time for color/fluorescence fading decreases. This observation is not unexpected since we have noted that the non-nucleophilic bases still have a certain degree of nucleophilicity; therefore, an excessive amount of base will accelerate the ring-opening process, resulting in more rapid self-destruction. In future work, we will conduct detailed and quantitative kinetic studies to explore how the amount of base added, the pH, and the nucleophilicity affect the halofluorochromic behavior of HA.

The mechanisms of the halofluorochromism and self-destruction of HA we reveal provide fresh insights into chemical and photophysical perspectives of the intriguing and versatile molecule, HA, deepen our understanding of six-membered anhydride rings with enolizable α-hydrogen(s) and the keto-enol tautomerism, and might inspire the molecular design strategy of dual-mode optical switching materials with tunable duration. By harnessing the halofluorochromism and self-destruction properties of HA and the duality of bases, we achieve controlled color and fluorescence duration and develop a CMY palette with unparalleled highly dynamic, multidimensional, and multimodal optical encryption capabilities. With the pH-responsive and self-destructive features, HA-derived systems hold unprecedented promise in constructing pH-responsive drug delivery systems owing to the diverse pH values of tissues at various physiological and pathological conditions. For future studies, it will also be of interest to expand the applications of HA and the CMY palette, as well as to design and develop more novel molecules and materials exhibiting halofluorochromism with a broader range of colors and dynamic features.

## MATERIALS AND METHODS

The methods and experimental details can be found in the Supplementary Materials.

## Supplementary Materials

**This PDF file includes:**

Supplementary Notes
Figs. S1 to S51
Tables S1 to S3
Materials and Methods
Legends for movies S1 to S4
References

**Other Supplementary Material for this manuscript includes the following:**

Movies S1 to S4

## REFERENCES AND NOTES


1. D. U. Andrews, B. R. Heazlewood, A. T. Maccarone, T. Conroy, R. J. Payne, M. J. T. Jordan, S. H. Kable, Photo-tautomerization of acetaldehyde to vinyl alcohol: A potential route to tropospheric acids. *Science* **337**, 1203–1206 (2012).
2. S. Liu, W. Yao, Y. Liu, Q. Wei, J. Chen, X. Wu, F. Xia, W. Hu, A Rh(II)-catalyzed multicomponent reaction by trapping an α-amino enol intermediate in a traditional two-component reaction pathway. *Sci. Adv.* **3**, e1602467 (2017).
3. A. SchÖNberg, A. Mustafa, W. Asker, Thermochromism and keto-enol tautomerism of solutions of 1:3-diketo-2-phenyl-5-bromoindan. *Nature* **171**, 222 (1953).
4. P. Zuman, J. Michl, Role of keto-enol tautomerism in the polarographical reduction of some carbonyl compounds. *Nature* **192**, 655–657 (1961).
5. B. R. Heazlewood, A. T. Maccarone, D. U. Andrews, D. L. Osborn, L. B. Harding, S. J. Klippenstein, M. J. T. Jordan, S. H. Kable, Near-threshold H/D exchange in CD3CHO photodissociation. *Nat. Chem.* **3**, 443–448 (2011).
6. C. Tang, T. Stuyver, T. Lu, J. Liu, Y. Ye, T. Gao, L. Lin, J. Zheng, W. Liu, J. Shi, S. Shaik, H. Xia, W. Hong, Voltage-driven control of single-molecule keto-enol equilibrium in a two-terminal junction system. *Nat. Commun.* **14**, 3657 (2023).
7. Y. Chiang, A. J. Kresge, Enols and other reactive species. *Science* **253**, 395–400 (1991).
8. P. Naumov, M. Kochunnoonny, Spectral–structural effects of the keto–enol–enolate and phenol–phenolate equilibria of oxyluciferin. *J. Am. Chem. Soc.* **132**, 11566–11579 (2010).
9. C. A. Taatjes, N. Hansen, A. McIlroy, J. A. Miller, J. P. Senosiain, S. J. Klippenstein, F. Qi, L. Sheng, Y. Zhang, T. A. Cool, J. Wang, P. R. Westmoreland, M. E. Law, T. Kasper, K. Kohse-Höinghaus, Enols are common intermediates in hydrocarbon oxidation. *Science* **308**, 1887–1889 (2005).
10. D. L. Boger, When sugar is not so sweet. *Science* **350**, 275–276 (2015).
11. C. Draghici, T. Wang, D. A. Spiegel, Concise total synthesis of glucosepane. *Science* **350**, 294–298 (2015).
12. T. A. Mollner, A. M. Giltrap, Y. Zeng, Y. Demyanenko, C. Buchanan, D. Oehlrich, A. J. Baldwin, D. C. Anthony, S. Mohammed, B. G. Davis, Reductive site-selective atypical *C,Z*-type/N2-C2 cleavage allows C-terminal protein amidation. *Sci. Adv.* **8**, eabl8675 (2022).
13. X. Zhang, E. King-Smith, L.-B. Dong, L.-C. Yang, J. D. Rudolf, B. Shen, H. Renata, Divergent synthesis of complex diterpenes through a hybrid oxidative approach. *Science* **369**, 799–806 (2020).
14. F. G. Cantú Reinhard, P. Barman, G. Mukherjee, J. Kumar, D. Kumar, D. Kumar, C. V. Sastri, S. P. de Visser, Keto–enol tautomerization triggers an electrophilic aldehyde deformylation reaction by a nonheme manganese(III)-peroxo complex. *J. Am. Chem. Soc.* **139**, 18328–18338 (2017).
15. N. Yoshikawa, Y. M. A. Yamada, J. Das, H. Sasai, M. Shibasaki, Direct catalytic asymmetric aldol reaction. *J. Am. Chem. Soc.* **121**, 4168–4178 (1999).

16. J. M. O'Connor, R. Uhrhammer, A. L. Rheingold, D. M. Roddick, Keto-enol tautomerization in metal-acyl complexes: The enolization properties of bimetallic .mu.-malonyl compounds. *J. Am. Chem. Soc.* **113**, 4530–4544 (1991).
17. D. A. Evans, J. S. Clark, R. Metternich, V. J. Novack, G. S. Sheppard, Diastereoselective aldol reactions using .beta.-keto imide derived enolates. A versatile approach to the assemblage of polypropionate systems. *J. Am. Chem. Soc.* **112**, 866–868 (1990).
18. F. Velazquez Escobar, P. Piwowarski, J. Salewski, N. Michael, M. Fernandez Lopez, A. Rupp, B. M. Qureshi, P. Scheerer, F. Bartl, N. Frankenberg-Dinkel, F. Siebert, M. Andrea Mroginski, P. Hildebrandt, A protonation-coupled feedback mechanism controls the signalling process in bathy phytochromes. *Nat. Chem.* **7**, 423–430 (2015).
19. W. T. Astbury, D. M. Wrinch, Intramolecular folding of proteins by keto-enol interchange. *Nature* **139**, 798 (1937).
20. S. Liu, S. Li, G. Shen, N. Sukumar, A. M. Krezel, W. Li, Structural basis of antagonizing the vitamin K catalytic cycle for anticoagulation. *Science* **371**, eabc5667 (2021).
21. S. Borsley, E. Kreidt, D. A. Leigh, B. M. W. Roberts, Autonomous fuelled directional rotation about a covalent single bond. *Nature* **604**, 80–85 (2022).
22. M. González-López, J. T. Shaw, Cyclic anhydrides in formal cycloadditions and multicomponent reactions. *Chem. Rev.* **109**, 164–189 (2009).
23. I. Atodiresei, I. Schiffers, C. Bolm, Stereoselective anhydride openings. *Chem. Rev.* **107**, 5683–5712 (2007).
24. G. Dey, A. Chakraborty, Tautomers of homophthalic anhydride in the ground and excited electronic states: Analysis through energy, hardness and vibrational signatures. *J. Mol. Model.* **26**, 173 (2020).
25. C. G. Seitz, H. Zhang, Y. Mo, J. M. Karty, Why do enolate anions favor O-alkylation over C-alkylation in the gas phase? The roles of resonance and inductive effects in the gas-phase SN2 reaction between the acetaldehyde enolate anion and methyl fluoride. *J. Org. Chem.* **81**, 3711–3719 (2016).
26. G. Moss, P. Smith, D. Tavernier, Glossary of class names of organic compounds and reactivity intermediates based on structure (IUPAC Recommendations 1995). *Pure Appl. Chem.* **67**, 1307–1375 (1995).
27. Y. Tamura, M. Sasho, K. Nakagawa, T. Tsugoshi, Y. Kita, Strong base induced cycloaddition of homophthalic anhydrides leading to peri-hydroxy polycyclic compounds. *J. Org. Chem.* **49**, 473–478 (1984).
28. Y. Tamura, A. Wada, M. Sasho, Y. Kita, Cycloaddition of homophthalic anhydride: A new and simple route to linearly condensed phenolic compoumds. *Tetrahedron Lett.* **22**, 4283–4286 (1981).
29. R. Jangir, "Homophthalic anhydride derivatives to bioactive natural products," thesis, CSIR-National Chemical Laboratory (2016).
30. J. Andréasson, U. Pischel, Molecules for security measures: From keypad locks to advanced communication protocols. *Chem. Soc. Rev.* **47**, 2266–2279 (2018).
31. S. Liu, X. Liu, J. Yuan, J. Bao, Multidimensional information encryption and storage: When the input is light. *Research* **2021**, 7897849 (2021).
32. S. A. Jenekhe, J. A. Osaheni, Excimers and exciplexes of conjugated polymers. *Science* **265**, 765–768 (1994).
33. G. Bünau, J. Birks, J. B. Birks: Photophysics of aromatic molecules. Wiley-Interscience, London 1970. 704 Seiten. Preis: 210s. *Ber. Bunsen. Phys. Chem* **74**, 1294–1295 (1970).
34. P. Sahu, M. Gupta, Water absorption behavior of cellulosic fibres polymer composites: A review on its effects and remedies. *J. Indust. Textiles* **51**, 7480S–7512S (2022).
35. S. Cichosz, A. Masek, IR study on cellulose with the varied moisture contents: Insight into the supramolecular structure. *Materials* **13**, 4573 (2020).
36. H. M. Akil, C. Santulli, F. Sarasini, J. Tirillò, T. Valente, Environmental effects on the mechanical behaviour of pultruded jute/glass fibre-reinforced polyester hybrid composites. *Compos. Sci. Technol.* **94**, 62–70 (2014).
37. Z. N. Azwa, B. F. Yousif, A. C. Manalo, W. Karunasena, A review on the degradability of polymeric composites based on natural fibres. *Mater. Des.* **47**, 424–442 (2013).
38. A.-M. Olsson, L. Salmén, The association of water to cellulose and hemicellulose in paper examined by FTIR spectroscopy. *Carbohydr. Res.* **339**, 813–818 (2004).
39. C. Würth, M. Grabolle, J. Pauli, M. Spieles, U. Resch-Genger, Relative and absolute determination of fluorescence quantum yields of transparent samples. *Nat. Protoc.* **8**, 1535–1550 (2013).
40. S. G. Khokarale, J.-P. Mikkola, Hydrogen sulfide gas capture by organic superbase 1,8-diazabicyclo-[5.4.0]-undec-7-ene through salt formation: Salt synthesis, characterization and application for $CO_2$ capture. *RSC Adv.* **8**, 18531–18541 (2018).
41. J. Song, Y. X. Lei, Z. Rappoport, The first solid enols of anhydrides. Structure, properties, and enol/anhydride equilibria. *J. Org. Chem.* **72**, 9152–9162 (2007).
42. N. E. Guedira, R. Beugelmans, Ambident behavior of ketone enolate anions in SNAr substitutions on fluorobenzonitrile substrates. *J. Org. Chem.* **57**, 5577–5585 (1992).
43. J. E. McMurry, *Organic Chemistry* (Cengage Learning, 2008).
44. R. Atta ur, M. I. Choudhary, W. Atia tul, Chapter 4—Spin-echo and polarization transfer, in *Solving Problems with NMR Spectroscopy (Second Edition)*, R. Atta ur, M. I. Choudhary, W. Atia tul, Eds. (Academic Press, 2016), pp. 133–190.
45. G. Gemmecker, H. Kessler, Chapter 2—Methodology and applications of heteronuclear and multidimensional $^{13}C$ NMR to the elucidation of molecular structure and dynamics in the liquid state, in *Carbon-13 NMR Spectroscopy of Biological Systems*, N. Beckmann, Ed. (Academic Press, 1995), pp. 7–64.
46. T. D. W. Claridge, Chapter 4—One-dimensional techniques, in *High-Resolution NMR Techniques in Organic Chemistry (Third Edition)*, T. D. W. Claridge, Ed. (Elsevier, 2016), pp. 133–169.
47. M. J. Frisch, G. W. Trucks, H. B. Schlegel, G. E. Scuseria, M. A. Robb, J. R. Cheeseman, G. Scalmani, V. Barone, G. A. Petersson, H. Nakatsuji, X. Li, M. Caricato, A. V. Marenich, J. Bloino, B. G. Janesko, R. Gomperts, B. Mennucci, H. P. Hratchian, J. V. Ortiz, A. F. Izmaylov, J. L. Sonnenberg, D. Williams-Young, F. Ding, F. Lipparini, F. Egidi, J. Goings, B. Peng, A. Petrone, T. Henderson, D. Ranasinghe, V. G. Zakrzewski, J. Gao, N. Rega, G. Zheng, W. Liang, M. Hada, M. Ehara, K. Toyota, R. Fukuda, J. Hasegawa, M. Ishida, T. Nakajima, Y. Honda, O. Kitao, H. Nakai, T. Vreven, K. Throssell, J. A. Montgomery, Jr., J. E. Peralta, F. Ogliaro, M. J. Bearpark, J. J. Heyd, E. N. Brothers, K. N. Kudin, V. N. Staroverov, T. A. Keith, R. Kobayashi, J. Normand, K. Raghavachari, A. P. Rendell, J. C. Burant, S. S. Iyengar, J. Tomasi, M. Cossi, J. M. Millam, M. Klene, C. Adamo, R. Cammi, J. W. Ochterski, R. L. Martin, K. Morokuma, O. Farkas, J. B. Foresman, D. J. Fox, *Gaussian 09, Revision E.01* (Gaussian Inc., 2013).
48. A. D. Becke, Density-functional thermochemistry. III. The role of exact exchange. *J. Chem. Phys.* **98**, 5648–5652 (1993).
49. C. Lee, W. Yang, R. G. Parr, Development of the Colle-Salvetti correlation-energy formula into a functional of the electron density. *Phys. Rev. B* **37**, 785–789 (1988).
50. F. Weigend, R. Ahlrichs, Balanced basis sets of split valence, triple zeta valence and quadruple zeta valence quality for H to Rn: Design and assessment of accuracy. *Phys. Chem. Chem. Phys.* **7**, 3297–3305 (2005).
51. F. Weigend, Accurate Coulomb-fitting basis sets for H to Rn. *Phys. Chem. Chem. Phys.* **8**, 1057–1065 (2006).
52. B. P. Pritchard, D. Altarawy, B. Didier, T. D. Gibson, T. L. Windus, New basis set exchange: An open, up-to-date resource for the molecular sciences community. *J. Chem. Inf. Model.* **59**, 4814–4820 (2019).
53. F. Furche, R. Ahlrichs, Adiabatic time-dependent density functional methods for excited state properties. *J. Chem. Phys.* **117**, 7433–7447 (2002).
54. J. Liu, W. Liang, Analytical Hessian of electronic excited states in time-dependent density functional theory with Tamm-Dancoff approximation. *J. Chem. Phys.* **135**, (2011).
55. T. Lu, F. Chen, Multiwfn: A multifunctional wavefunction analyzer. *J. Comput. Chem.* **33**, 580–592 (2012).
56. W. Humphrey, A. Dalke, K. Schulten, VMD: Visual molecular dynamics. *J. Mol. Graph.* **14**, 33–38 (1996).
57. E. Cancès, B. Mennucci, J. Tomasi, A new integral equation formalism for the polarizable continuum model: Theoretical background and applications to isotropic and anisotropic dielectrics. *J. Chem. Phys.* **107**, 3032–3041 (1997).
58. B. Mennucci, E. Cancès, J. Tomasi, Evaluation of solvent effects in isotropic and anisotropic dielectrics and in ionic solutions with a unified integral equation method: Theoretical bases, computational implementation, and mumerical applications. *J. Phys. Chem. B* **101**, 10506–10517 (1997).
59. F. Hutmacher, Why is there so much more research on vision than on any other sensory modality? *Front. Psychol.* **10**, 2246 (2019).
60. S. Hecht, S. Shlaer, M. H. Pirenne, Energy, quanta, and vision. *J. Gen. Physiol.* **25**, 819–840 (1942).
61. D. A. Baylor, T. Lamb, K.-W. Yau, Responses of retinal rods to single photons. *J. Physiol.* **288**, 613–634 (1979).
62. G. Wald, Human vision and the spectrum. *Science* **101**, 653–658 (1945).
63. T. Ebrey, Y. Koutalos, Vertebrate photoreceptors. *Prog. Retin. Eye Res.* **20**, 49–94 (2001).
64. J. K. Bowmaker, H. Dartnall, Visual pigments of rods and cones in a human retina. *J. Physiol.* **298**, 501–511 (1980).
65. S. Newton, *Opticks: Or, A Treatise of the Reflexions, Refractions, Inflexions and Colours of Light. Also Two Treaties of the Species and Magnitude of Curvilinear Figures. [The Advertisement Signed: IN, Ie Sir Isaac Newton]* (Sam. Smith & Benj. Walford, 1704).
66. H. v. Helmholtz, Über die Theorie der zusammengesetzten Farben. *Ann. Phys.* **163**, 45–66 (1852).
67. H. Grassmann, XXXVII. On the theory of compound colours. *Philos. Mag.* **7**, 254–264 (1854).
68. B. G. von Rumford, *The Complete Works of Count Rumford* (Macmillan, 1876), vol. 1.
69. J. C. Maxwell IV, On the theory of compound colours, and the relations of the colours of the spectrum. *Philos. Trans. R. Soc.* **150**, 57–84 (1860).
70. E. C. Carter, J. D. Schanda, R. Hirschler, S. Jost, M. R. Luo, M. Melgosa, Y. Ohno, M. R. Pointer, D. C. Rich, F. Viénot, L. Whitehead, J. H. Wold, "Colorimetry, 4th Edition" (Tech. Rep. Commission Internationale de l'Eclairage CIE 015: 2018).
71. G. Wyszecki, W. S. Stiles, *Color Science* (Wiley, 1982), vol. 8.
72. R. W. Pridmore, Complementary colors: A literature review. *Color Res. Appl.* **46**, 482–488 (2021).

73. R. W. Sabnis, Phthalein dyes, in *Kirk-Othmer Encyclopedia of Chemical Technology* (Wiley, 1978), pp. 1–21.
74. C. CIE, *Commission internationale de l'eclairage proceedings, 1931* (Cambridge University, 1932).
75. T. Smith, J. Guild, The CIE colorimetric standards and their use. *Trans. Opt. Soc.* **33**, 73 (1932).
76. W. D. Wright, A re-determination of the trichromatic coefficients of the spectral colours. *Trans. Opt. Soc.* **30**, 141 (1929).
77. J. Guild, The colorimetric properties of the spectrum. *Philos. Trans. R. Soc. Lond. A* **230**, 149–187 (1931).
78. R. W. G. Hunt, M. R. Pointer, *Measuring Colour* (John Wiley & Sons, 2011).
79. Aminomethyl Propanol, https://www.cosmeticsinfo.org/ingredients/aminomethyl-propanol/ (2024).
80. G. M. Sheldrick, SHELXT–Integrated space-group and crystal-structure determination. *Acta Crystallogr. A Found. Adv.* **71**, 3–8 (2015).
81. O. V. Dolomanov, L. J. Bourhis, R. J. Gildea, J. A. Howard, H. Puschmann, OLEX2: A complete structure solution, refinement and analysis program. *J. Appl. Cryst.* **42**, 339–341 (2009).
82. C. Würth, M. Grabolle, J. Pauli, M. Spieles, U. Resch-Genger, Comparison of methods and achievable uncertainties for the relative and absolute measurement of photoluminescence quantum yields. *Anal. Chem.* **83**, 3431–3439 (2011).


**Acknowledgments:** We thank T. Mal and C. George from the Pennsylvania State University for guidance on NMR measurements, Q. Liu from the Ohio State University and F. Hao from the Pennsylvania State University for helpful suggestions on NMR data analyses, H. Yennawar from the Pennsylvania State University for help on single-crystal x-ray diffraction analysis (the x-ray system at Penn State Huck X-ray Crystallography and Automated Biological Calorimetry Core Facilities is supported by National Institutes of Health awards 1S10OD028589-01 and 1S10RR023439-01 to N. Yennawar), Y. Liang from the Pennsylvania State University for help on smartphone app development, T. Xia from the Pennsylvania State University for help on CMY gamut simulation, Q. Wang and Y. Zhou from the Pennsylvania State University for letting us use the glovebox, and Y. Chen from Instrumentation and Service Center for Molecular Sciences at Westlake University for the assistance in HR-MS measurement. **Funding:** Y.W. and L.-Q.C. acknowledge the generous support from the Hamer Foundation through the Hamer Professorship at Penn State. **Author contributions:** D.W. and J.Y. conceived the project; D.W. performed most of the experiments, analyzed the data, and prepared the draft of the manuscript; Y.W. performed DFT calculations; T.J.Z. performed the FTIR measurements and analyzed the FTIR data; L.-Q.C. gave suggestions on the DFT calculations; and J.Y. supervised the project. All authors revised and contributed to the final version of the manuscript. **Competing interests:** The authors declare that they have no competing interests. **Data and materials availability:** All data needed to evaluate the conclusions in the paper are present in the paper and/or the Supplementary Materials. Crystallographic data for the keto form of homophthalic anhydride ($HA_k$) and homophthalic acid are available from the Cambridge Crystallographic Data Center under reference numbers CCDC 2206140 and 2206139, respectively. Code for color gamut simulation and anti-counterfeiting app are archived in Zenodo (doi: 10.5281/zenodo.10890981 and doi: 10.5281/zenodo.10891005, respectively).

Submitted 9 January 2024
Accepted 12 April 2024
Published 17 May 2024
10.1126/sciadv.adn9692